Final Accepted Version

Contents lists available at ScienceDirect

Chinese Journal of Aeronautics

journal homepage: www.elsevier.com/locate/cja

Docking control for probe-drogue refueling: An additive-state-decomposition-based output feedback iterative learning control method

Jinrui REN [a,b], Quan QUAN[a,*], Cunjia LIU [b], Kai-Yuan CAI [a]

[a]*School of Automation Science and Electrical Engineering, Beihang University, Beijing 100083, China*
[b]*Department of Aeronautical and Automotive Engineering, Loughborough University, Leicestershire, LE11 3TU, United Kingdom*

Received 13 March 2019; revised 5 August 2019; accepted 29 October 2019

Abstract

Designing a controller for the docking maneuver in Probe-Drogue Refueling (PDR) is an important but challenging task, due to the complex system model and the high precision requirement. In order to overcome the disadvantage of only feedback control, a feedforward control scheme known as Iterative Learning Control (ILC) is adopted in this paper. First, Additive State Decomposition (ASD) is used to address the tight coupling of input saturation, nonlinearity and the property of NonMinimum Phase (NMP) by separating these features into two subsystems (a primary system and a secondary system). After system decomposition, an adjoint-type ILC is applied to the Linear Time-Invariant (LTI) primary system with NMP to achieve entire output trajectory tracking, whereas state feedback is used to stabilize the secondary system with input saturation. The two controllers designed for the two subsystems can be combined to achieve the original control goal of the PDR system. Furthermore, to compensate for the receiver-independent uncertainties, a correction action is proposed by using the terminal docking error, which can lead to a smaller docking error at the docking moment. Simulation tests have been carried out to demonstrate the performance of the proposed control method, which has some advantages over the traditional derivative-type ILC and adjoint-type ILC in the docking control of PDR.

Keywords: Probe-drogue refueling; Docking control; Iterative learning control; Adjoint operator; Additive state decomposition; Stable inversion;

1. Introduction

Autonomous Aerial Refueling (AAR) is an important method to increase the voyage and endurance of Unmanned Aerial Vehicles (UAVs) and avoid the conflict between the takeoff weight and the payload weight[1,2]. Among the aerial refueling methods in operation today, the Probe-Drogue Refueling (PDR)[3] is the most widely adopted one owing to its flexibility and simple requirement for equipment. There are five stages in the process of PDR, and docking is the most critical and difficult stage because it is more susceptible to disturbances, which directly affects the success of AAR. The docking control task is to control the probe on the receiver to link up with the drogue for fuel transfer. The

*Corresponding author. *E-mail address:* qq_buaa@buaa.edu.cn

docking control for PDR is a difficult task for two main reasons. First, the system model in the docking stage is a Multi-Input-Multi-Output (MIMO) higher-order nonlinear system with nonminimum-phase, multi-agent, and multi-disturbance features, which is complex for control design. Moreover, the receiver dynamics is slower than the motion of the drogue, and so it is hard for the probe on the receiver to capture the moving drogue. The second reason is that the precision requirement for the PDR docking control is high. Concretely, the docking error should be controlled within the centimeter level, and the relative velocity between the probe and the drogue should be controlled within a small range, such as 1.0-1.5 m/s[1,4]. Therefore, the docking controller design for PDR is important but challenging.

Most existing docking control methods for PDR mainly focus on feedback control, such as Linear Quadratic Regulator (LQR)[5,6], NonZero SetPoint (NZSP)[7,8], Active Disturbance Rejection Control (ADRC)[9], adaptive control[10,11], backstepping control[12,13], etc. Feedback control methods are likely to result in a chasing process between the receiver and the drogue, which may cause overcontrol. Besides, the chasing action may lead to certain impact and damage to the drogue and the probe, which is dangerous and needs to be avoided according to ATP-56(B) issued by NATO (North Atlantic Treaty Organisation) [4]. Under this circumstance, Iterative Learning Control (ILC) attracts the researchers' attention. ILC[14] is an effective cycle-to-cycle feedforward control approach to achieve entire output trajectory tracking within a given time interval. It often applies to systems that repeat the same operation over a finite trial length $0 \le t \le T$. The repeatability of the considered system can be utilized to improve the system control performance via the ILC method. For the docking of the PDR system, if a docking attempt fails, the receiver will retreat to the standby position for the next attempt, as shown in Fig. 1, where k is the cycle number. That means the docking process is repetitive. Thus, ILC is a good choice to solve the docking control problem[15].

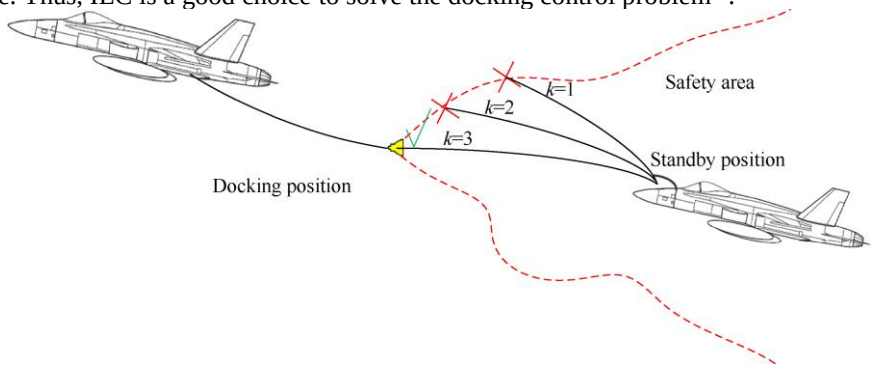

Fig. 1 Repetitive docking operation in aerial refueling.

The tool of system inversion plays a crucial role in the classical ILC design to approach perfect tracking[16]. However, for a NonMinimum Phase (NMP) system, the common system inversion is unstable. Thus, many special ILC designs for NMP systems were proposed. Stable inversion is a non-causal method to solve the tracking problem for NMP systems[17,18] by avoiding the influence of the unstable zeros of the system. However, completely accurate information about the system is required. Therefore, if there exists any uncertainty about the system, then the conventional stable inversion method cannot be applied directly[19]. Based on the stable inversion, an adjoint-type ILC is proposed[20-26], which employs the adjoint operator to make the input to approach the stable inversion[19]. Because of its online iterative process, the controller can deal with uncertainties, and obtain a better tracking result than that obtained by the conventional stable inversion method.

Because the receiver dynamics is a typical NMP system, PDR systems are a class of nonminimum phase nonlinear systems with input saturation, and the main difficulty of solving the docking control problem for PDR is caused by the tight coupling of input saturation, nonlinearity and the property of NMP. There are some mature methods to deal with these features separately. However, for the systems with all the three features coupled, adopting existing methods may lead to complex computation and low convergence speed. For docking control, it is expected that the docking should be completed as quickly as possible, for example within 2-3 docking attempts. In order to address the problem, a method called Additive-State-Decomposition-Based (ASDB) ILC is proposed in this work. Through Additive State Decomposition[27,28] (ASD), a kind of system separation method, the influence of NMP is separated to a subsystem named primary system, and the input saturation and nonlinearity features are left to the other subsystem named secondary system. Then, designing controllers for these two subsystems is easier than designing a controller for the original PDR system.

In this work, how to adjust fast among different tasks in PDR to achieve a successful docking is focused. Uncertainties among different tasks can be divided into two parts. One part is caused by the state change of the receiver, e.g., the mass change because of the fuel change, or the system matrix change because of a different trimming state. The other part is the uncertainty from receiver-independent reasons, e.g., atmospheric environment change, the bow

wave change owing to the change of air density, and the change of the refueling equipment. According to these two kinds of uncertainties, two steps are included in the controller design. First, based on ASD and adjoint operator, ILC controller is designed to attenuate the receiver-related uncertainty. Entire output trajectory tracking can be achieved. Then, a correction action is proposed by using the ultimate docking error. Because only a single-point error is used, entire output trajectory tracking cannot be achieved, but the influence of the receiver-independent uncertainty can be eliminated.

The contributions of this work are as follows:

1) The input saturation and nonlinearity features are separated from the NMP feature by ASD, and then the NMP feature is addressed by using the adjoint-type ILC, which makes the adjoint-type ILC applicable to the nonlinear PDR system in an indirect way.

2) Fast adjustment among different tasks in the docking control for PDR is accomplished, and uncertainties among different tasks can be eliminated.

The notations used in this paper are summarized in Table 1.

Table 1 Definition of some functional notations.

Functional notation	Meaning
$\|\boldsymbol{\alpha}\| = \sqrt{\boldsymbol{\alpha}^{\mathrm{T}}\boldsymbol{\alpha}}$	2-norm of a vector $\boldsymbol{\alpha}$
$\|\boldsymbol{\alpha}\|_{\mathcal{L}_2[t_1,t_2]} = \sqrt{\int_{t_1}^{t_2} \boldsymbol{\alpha}^{\mathrm{T}}(t)\boldsymbol{\alpha}(t)\mathrm{d}t}$	$\mathcal{L}_2$ norm of a functional vector $\boldsymbol{\alpha}$ defined on $t \in [t_1, t_2]$
$\langle \boldsymbol{\alpha}_1, \boldsymbol{\alpha}_2 \rangle_{\mathcal{L}_2[t_1,t_2]} = \sqrt{\int_{t_1}^{t_2} \boldsymbol{\alpha}_1^{\mathrm{T}}(t)\boldsymbol{\alpha}_2(t)\mathrm{d}t}$	Inner product of functional vectors $\boldsymbol{\alpha}_1, \boldsymbol{\alpha}_2$ defined on $t \in [t_1, t_2]$
$\|\boldsymbol{\alpha}\|_{\mathcal{L}_\infty[t_1,t_2]} = \sup_{t\in[t_1,t_2]} \|\boldsymbol{\alpha}(t)\|$	$\mathcal{L}_\infty$ norm of a functional vector $\boldsymbol{\alpha}$ defined on $t \in [t_1, t_2]$
$\|\mathcal{G}\|_{\mathcal{L}_2[t_1,t_2]} = \sup_{\|x\|_{\mathcal{L}_2[t_1,t_2]}\le 1} \|\mathcal{G}x\|_{\mathcal{L}_2[t_1,t_2]}$	Operator norm of an operator $\mathcal{G}$ defined on $t \in [t_1, t_2]$, which is compatible with $\mathcal{L}_2$ norm
$\mathcal{G}^*, \langle y, \mathcal{G}u \rangle = \langle \mathcal{G}^* y, u \rangle$	Adjoint operator of an operator $\mathcal{G}$

2. System description and problem formulation

2.1. PDR system model in docking stage

Figs. 2-3 show the PDR system, which consists of a tanker aircraft with a flexible hose that trails behind and below the tanker, a cone-shaped drogue mounted at the end of the hose, and a receiver aircraft equipped with a rigid probe protruding from its nose. The docking control task for the receiver aircraft is to close with the tanker and dock the fuel probe tip with the drogue receptacle. When establishing the PDR system model in the docking stage, three commonly used coordinate frames are the ground frame (o_g-$x_g y_g z_g$), the tanker frame (o_t-$x_t y_t z_t$), and the drogue equilibrium-point frame (o_d-$x_d y_d z_d$), which are shown in Fig. 2. In Fig. 2, h_t^g denotes the flight height of the tanker in the ground frame and v_t^g is the forward flight velocity of the tanker in the ground frame. The formal definition of these coordinate frames can be found in Ref.[29].

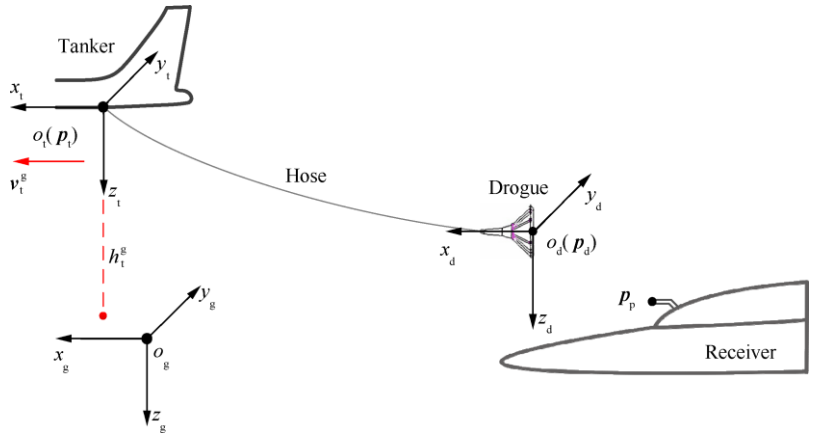

Fig. 2 Coordinate frames for PDR system.

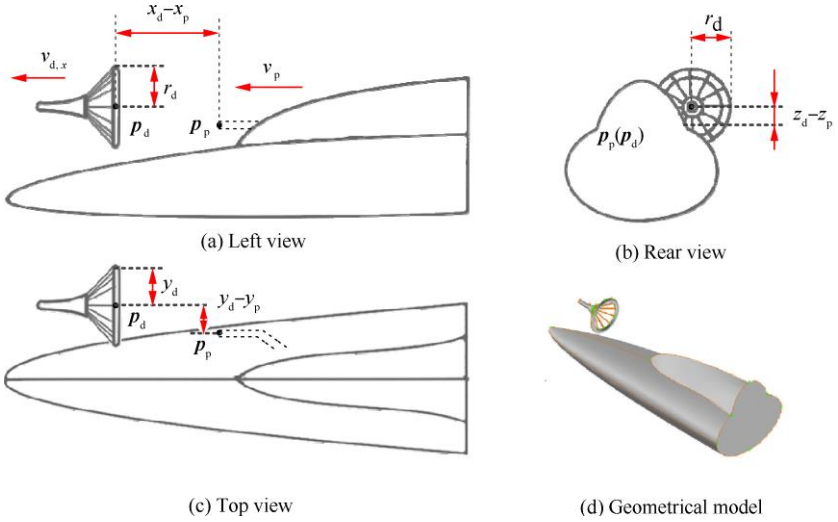

Fig. 3 Three views of PDR system.

During the docking stage, the receiver aircraft is the one that is controllable and to be controlled. Thus, the receiver model[30] (F-16 aircraft is considered) is given first. In practice, the receiver model is often decoupled into longitudinal and lateral channels. Taking the Stability Augmentation Control (SAC) into account (often adopted for the receiver to place the poles of the receiver system to reasonable positions in the left-half s-plane), the receiver with SAC is represented as

$$\begin{cases} \underbrace{\begin{bmatrix} \dot{\boldsymbol{x}}_{\text{rlong}} \\ \dot{\boldsymbol{x}}_{\text{rlat}} \end{bmatrix}}_{\dot{\boldsymbol{x}}_{\text{r}}} = \underbrace{\begin{bmatrix} \boldsymbol{A}_{\text{rlong}} & \boldsymbol{0} \\ \boldsymbol{0} & \boldsymbol{A}_{\text{rlat}} \end{bmatrix}}_{\boldsymbol{A}_{\text{r}}} \underbrace{\begin{bmatrix} \boldsymbol{x}_{\text{rlong}} \\ \boldsymbol{x}_{\text{rlat}} \end{bmatrix}}_{\boldsymbol{x}_{\text{r}}} + \underbrace{\begin{bmatrix} \boldsymbol{B}_{\text{rlong},1} & \boldsymbol{0} & \boldsymbol{B}_{\text{rlong},2} \\ \boldsymbol{0} & \boldsymbol{B}_{\text{rlat},1} & \boldsymbol{0} \end{bmatrix}}_{\boldsymbol{B}_{\text{r}}} \text{sat}\left(\boldsymbol{u}_{\text{r}}\right) \\ \underset{\boldsymbol{y}_{\text{r}}}{\boldsymbol{p}_{\text{r}}} = \underbrace{\begin{bmatrix} \boldsymbol{C}_{\text{rlong},1} & \boldsymbol{0} \\ \boldsymbol{0} & \boldsymbol{C}_{\text{rlat},1} \\ \boldsymbol{C}_{\text{rlong},2} & \boldsymbol{0} \end{bmatrix}}_{\boldsymbol{C}_{\text{r}}} \underbrace{\begin{bmatrix} \boldsymbol{x}_{\text{rlong}} \\ \boldsymbol{x}_{\text{rlat}} \end{bmatrix}}_{\boldsymbol{x}_{\text{r}}} \end{cases} \tag{1}$$

Where $\boldsymbol{p}_{\text{r}} \triangleq \begin{bmatrix} x_{\text{r}} & y_{\text{r}} & z_{\text{r}} \end{bmatrix}^{\text{T}}$, $\boldsymbol{u}_{\text{r}} \triangleq \begin{bmatrix} u_{\delta_{\text{T}}} & u_{\delta_{\text{a}}} & u_{\delta_{\text{e}}} \end{bmatrix}^{\text{T}}$ is the control input of throttle, aileron, and elevator from the low-level control, the subscript r denotes the receiver, the subscript long or lat refers to the longitudinal or lateral channel, the subscript 1 or 2 means the first or second column of the input matrix, or the first or second row of the output matrix (the rudder input in the lateral channel is set to zero to solve the overactuation problem). Note that, all the system matrices $\boldsymbol{A}_{\text{rlong}}$, $\boldsymbol{A}_{\text{rlat}}$, $\boldsymbol{B}_{\text{rlong},1}$, $\boldsymbol{B}_{\text{rlong},2}$, $\boldsymbol{B}_{\text{rlat},1}$, $\boldsymbol{C}_{\text{rlong},1}$, $\boldsymbol{C}_{\text{rlong},2}$, $\boldsymbol{C}_{\text{rlat},1}$ are known time-invariant matrices with appropriate dimensions. The function $\text{sat}(\bullet)$ is a saturation function defined as

$$\mathrm{sat}\left(\boldsymbol{u}\left(t\right)\right)=\begin{cases}u_{i,\min} & u_i\left(t\right)<u_{i,\min}\\ u_i\left(t\right) & u_{i,\min}<u_i\left(t\right)<u_{i,\max}\\ u_{i,\max} & u_i\left(t\right)>u_{i,\max}\end{cases};\boldsymbol{u}\left(t\right)=\left[u_1,u_2,\cdots u_i,\cdots u_n\right]^{\mathrm{T}} \tag{2}$$

Based on the receiver model (1), the probe position is determined by

$$\boldsymbol{p}_{\mathrm{p}}=\boldsymbol{p}_{\mathrm{r}}+\boldsymbol{p}_{\mathrm{p/r}} \tag{3}$$

where $\boldsymbol{p}_{\mathrm{p/r}}$ is the distance from the receiver to the probe.

The tracking object of the receiver is the drogue. According to Ref.[29], the drogue dynamics is expressed by a transfer function, for which the corresponding state-space representation is

$$\begin{cases}\dot{\boldsymbol{x}}_{\mathrm{d}}=\boldsymbol{A}_{\mathrm{d}}\boldsymbol{x}_{\mathrm{d}}+\boldsymbol{B}_{\mathrm{d}}\boldsymbol{f}_{\mathrm{b}}\\ \boldsymbol{p}_{\mathrm{d}}=\boldsymbol{C}_{\mathrm{d}}\boldsymbol{x}_{\mathrm{d}}\end{cases} \tag{4}$$

where the subscript d stands for the drogue, $\boldsymbol{p}_{\mathrm{d}}=\left[x_{\mathrm{d}}\quad y_{\mathrm{d}}\quad z_{\mathrm{d}}\right]^{\mathrm{T}}$ is the position of the drogue under the tanker frame, $\boldsymbol{x}_{\mathrm{d}}\in\mathbf{R}^{10}$ is the state of the drogue, for which the dimension is determined by the order of the fitting model in the identification, the input $\boldsymbol{f}_{\mathrm{b}}\in\mathbf{R}^3$ is the bow wave effect force acting on the drogue. Similar to the receiver model, all the system matrices $\boldsymbol{A}_{\mathrm{d}}$, $\boldsymbol{B}_{\mathrm{d}}$, $\boldsymbol{C}_{\mathrm{d}}$ are time-invariant and of appropriate dimensions. Furthermore, the bow wave effect can be represented by a nonlinear function[29]

$$\boldsymbol{f}_{\mathrm{b}}\triangleq\phi_0\left(\boldsymbol{p}_{\mathrm{d}}-\boldsymbol{p}_{\mathrm{r}}\right) \tag{5}$$

Apart from the input force from the receiver bow wave $\boldsymbol{f}_{\mathrm{b}}$, there are no other control inputs in the drogue dynamics (4). Therefore, the drogue dynamics is uncontrollable and the drogue position passively affected by the aerodynamic disturbances from the receiver (in a close range) and the atmospheric environment.

On the whole, by combining Eqs. (1), (3), (4), and (5), a comprehensive model for the PDR system is described as

$$\begin{cases}\underbrace{\begin{bmatrix}\dot{\boldsymbol{x}}_{\mathrm{d}}\\ \dot{\boldsymbol{x}}_{\mathrm{r}}\end{bmatrix}}_{\dot{\boldsymbol{x}}}=\underbrace{\begin{bmatrix}\boldsymbol{A}_{\mathrm{d}} & \boldsymbol{0}\\ \boldsymbol{0} & \boldsymbol{A}_{\mathrm{r}}\end{bmatrix}}_{\boldsymbol{A}}\underbrace{\begin{bmatrix}\boldsymbol{x}_{\mathrm{d}}\\ \boldsymbol{x}_{\mathrm{r}}\end{bmatrix}}_{\boldsymbol{x}}+\underbrace{\begin{bmatrix}\boldsymbol{B}_{\mathrm{d}}\phi_0\left(\boldsymbol{p}_{\mathrm{d}}-\boldsymbol{p}_{\mathrm{r}}\right)\\ \boldsymbol{0}\end{bmatrix}}_{\phi(y)}+\underbrace{\begin{bmatrix}\boldsymbol{0}\\ \boldsymbol{B}_{\mathrm{r}}\end{bmatrix}}_{\boldsymbol{B}}\mathrm{sat}\left(\boldsymbol{u}_{\mathrm{r}}\right)\\ \underbrace{\left[\boldsymbol{p}_{\mathrm{d}}-\boldsymbol{p}_{\mathrm{p}}\right]}_{\boldsymbol{y}}=\underbrace{\left[\boldsymbol{C}_{\mathrm{d}}\quad-\boldsymbol{C}_{\mathrm{r}}\right]}_{\boldsymbol{C}}\underbrace{\begin{bmatrix}\boldsymbol{x}_{\mathrm{d}}\\ \boldsymbol{x}_{\mathrm{r}}\end{bmatrix}}_{\boldsymbol{x}}-\boldsymbol{p}_{\mathrm{p/r}}\end{cases} \tag{6}$$

During the docking stage, the docking moment is defined as

$$t_{\mathrm{dock}}=\arg\min_{t}\left|x_{\mathrm{d}}\left(t\right)-x_{\mathrm{p}}\left(t\right)\right| \tag{7}$$

If

$$\begin{gathered}\sqrt{\left(y_{\mathrm{d}}^{t_{\mathrm{dock}}}-y_{\mathrm{p}}^{t_{\mathrm{dock}}}\right)^2+\left(z_{\mathrm{d}}^{t_{\mathrm{dock}}}-z_{\mathrm{p}}^{t_{\mathrm{dock}}}\right)^2}\le r_{\mathrm{d}}\\ -v_{\max}<v_{\mathrm{d},x}^{t_{\mathrm{dock}}}-v_{\mathrm{p}}^{t_{\mathrm{dock}}}<-v_{\min}\end{gathered} \tag{8}$$

then the docking is viewed as successful, where $v_{\mathrm{d},x}\in\mathbf{R}$ is the drogue velocity in the direction of the x axis of the tanker frame $o_{\mathrm{t}}x_{\mathrm{t}}$, $v_{\mathrm{p}}\in\mathbf{R}$ is the velocity of the front-end of the probe, $v_{\max},v_{\min}$ are the threshold of relative velocity to open the fuel valve at the docking moment, and r_{d} is the radius of the drogue as shown in Fig. 3.

2.2. ILC problem statement

According to Section 1, ILC is a preferable way to solve the docking control problem. A comprehensive model for the PDR system is described as Eq. (6). For PDR systems, the drogue dynamics is passive and uncontrollable. Thus, the receiver aircraft (1) is focused and rewritten as a model for ILC controller design:

$$\begin{cases}\dot{\boldsymbol{x}}_{\mathrm{r},k}\left(t\right)=\boldsymbol{A}_{\mathrm{r}}\boldsymbol{x}_{\mathrm{r},k}\left(t\right)+\boldsymbol{B}_{\mathrm{r}}\mathrm{sat}\left(\boldsymbol{u}_{\mathrm{r},k}\left(t\right)\right)\\ \boldsymbol{y}_{\mathrm{r},k}\left(t\right)=\boldsymbol{C}_{\mathrm{r}}\boldsymbol{x}_{\mathrm{r},k}\left(t\right)\end{cases}\qquad\boldsymbol{x}_{\mathrm{r},k}\left(0\right)=\boldsymbol{x}_{\mathrm{r},0};t\in\left[0,T\right] \tag{9}$$

where $t \in [0 \quad T]$ is the time with the cycle period T, the subscript $k \in \mathbf{N}^+$ is the cycle number. The system matrix $\boldsymbol{A}_{\mathrm{r}}$ is stable, system (9) is a nonminimum-phase nonlinear system with input saturation, and its relative order is r, $\boldsymbol{x}_{\mathrm{r},0}$ represents the initial condition, which can be measured by various types of sensors, for example, vision-based systems. The following preliminary assumptions are made on system (9).

Assumption 1. The reference trajectory $\boldsymbol{y}_{\mathrm{r,d}}$ satisfies

$$\frac{\mathrm{d}^r \boldsymbol{y}_{\mathrm{r,d}}}{\mathrm{d}t^r} \in \mathcal{L}_\infty [0, T] \tag{10}$$

Assumption 2. There exists a $\boldsymbol{u}_{\mathrm{r,d}} = \left[u_{\mathrm{r,d},1}, u_{\mathrm{r,d},2}, u_{\mathrm{r,d},3}\right]^{\mathrm{T}}$ such that $\boldsymbol{u}_{\mathrm{r}} = \boldsymbol{u}_{\mathrm{r,d}}$ makes $\boldsymbol{y}_{\mathrm{r}} = \boldsymbol{y}_{\mathrm{r,d}}$, where $u_{i,\min} < u_{\mathrm{r,d},i}(t) < u_{i,\max}$ $(i = 1,2,3)$ on $[0 \quad T]$.

Control objective. Construct a sequence of control $\boldsymbol{u}_{\mathrm{r},k}(t)$ for system (9), such that

$$\left\| \boldsymbol{y}_{\mathrm{r,d}}(t) - \boldsymbol{y}_{\mathrm{r},k}(t) \right\|_{\mathcal{L}_\infty [0,T]} \to 0, \text{as } k \to \infty \tag{11}$$

where $\boldsymbol{y}_{\mathrm{r},k}(t)$ is the corresponding output driven by $\boldsymbol{u}_{\mathrm{r},k}(t)$.

Remark 1. Assumption 2 means that there exists a desired input $\boldsymbol{u}_{\mathrm{r,d}}$ within the actuating ability of actuators. If such an input $\boldsymbol{u}_{\mathrm{r,d}}$ does not exist, then the desired output cannot be achieved and needs to be redesigned.

Remark 2. Assumption 1 is a necessary condition of Assumption 2, because, in the process of system inversion, the r-order time derivative of the reference trajectory $\boldsymbol{y}_{\mathrm{r,d}}$ needs to be calculated. If $\boldsymbol{y}_{\mathrm{r,d}}$ is not smooth enough, then the derivative will become infinite, and leads to that $u_{i,\min} < u_{\mathrm{r,d},i}(t) < u_{i,\max}$ $(i = 1,2,3)$ does not hold.

Remark 3. Although the proposed method in this paper requires that the system information, namely the matrices $\boldsymbol{A}_{\mathrm{r}}, \boldsymbol{B}_{\mathrm{r}}, \boldsymbol{C}_{\mathrm{r}}$ are known, it is an online iterative method, and it can deal with the system uncertainties. The system output can converge to the reference trajectory quickly even when there exist uncertainties. The simulation results in Section 4 will show the details.

For an actual PDR system, the drogue position and the relative position between the probe and the drogue are usually measured by vision-based sensors[31,32] whose measurement precision depends on the relative distance (higher precision in the closer distance). Therefore, compared with the trajectory data, the terminal positions of the probe and the drogue are usually easier to measure in practice. Filters can also be used to remove the sensor noise.

Noteworthy, the reference trajectory $\boldsymbol{y}_{\mathrm{r,d}}(t)$ and the initial iterative input $\boldsymbol{u}_{\mathrm{r},1}(t)$ can be achieved from historical experience (previous tasks), or through some theoretical methods including low-pass filter method[33], polynomial interpolation method[6], terminal guidance method[34], and iterative optimization method.

3. ASDB ILC controller design

In order to cope with the uncertainty from receiver-related and receiver-independent reasons, the controller design is divided into two steps. The first step is to design an ILC controller for the receiver system (9) based on ASD and adjoint operator. The second step is to introduce a correction term based on adjoint operator and integrated system (6). The receiver-related uncertainties can be diminished in the first step, while the receiver-independent uncertainties can be attenuated in the second step.

3.1. ILC based on ASD and adjoint operator

In this part, only the receiver is considered. By using ASD[27,28], the considered NMP nonlinear system (9) is decomposed into two systems: an NMP LTI system (12) as the primary system, together with a nonlinear system (15) with input saturation as the secondary system. Since the output of the primary system and the state of the secondary system can be observed, the original ILC problem for system (9) is correspondingly decomposed into two subproblems: an output feedback ILC problem for an NMP LTI system and a state feedback stabilization problem for a nonlinear system with input saturation. Thanks to the ASD, the ILC problem is independent of nonlinearity and input saturation. As a result, the two new subproblems are much easier than the original problem for the nonlinear NMP system with input saturation.

3.1.1. ASD for the receiver

Additive State Decomposition (ASD) is a decomposition method for nonlinear systems just like the superposition principle for linear systems. It aims to decompose a nonlinear system into a linear system (denoted as a primary system) and a nonlinear system (denoted as a secondary system). The basic idea is that the primary linear system describes the dynamics of the original system in the neighborhood of the desired operating point or commanded trajectory, and the secondary nonlinear system is obtained by subtracting the primary system from the original system. The decomposed two systems have the same dimension as the original system. The nonlinearity property is allocated to the secondary system and the tracking task is assigned to the primary system, which makes the controller design more flexible and easier. For general nonlinear time-invariant systems, the ASD procedure is similar to that in the paper[27,28]. For general nonlinear time-varying systems, the decomposed two systems are a linear time-varying system and a nonlinear time-varying system[35]. The corresponding ASD procedure is also similar to that in the paper. ASD has been applied in some other applications in our previous papers, and readers can refer to Ref.[27,28,35] for more details. In the following, ASD is introduced to decompose the aforementioned receiver aircraft model into two subsystems to make the following ILC controller design more flexible and easier.

ASD is applied to system (9). The primary system is chosen as

$$\begin{cases} \dot{\boldsymbol{x}}_{\mathrm{r},k}^{\mathrm{p}} = \boldsymbol{A}_{\mathrm{r}} \boldsymbol{x}_{\mathrm{r},k}^{\mathrm{p}} + \boldsymbol{B}_{\mathrm{r}} \boldsymbol{u}_{\mathrm{r},k}^{\mathrm{p}} \\ \boldsymbol{y}_{\mathrm{r},k}^{\mathrm{p}} = \boldsymbol{C}_{\mathrm{r}} \boldsymbol{x}_{\mathrm{r},k}^{\mathrm{p}}, \boldsymbol{x}_{\mathrm{r},k}^{\mathrm{p}}(0) = \boldsymbol{x}_{\mathrm{r},0} \end{cases} \tag{12}$$

which is a three-input-three-output linear system. Then, by subtracting the primary system (12) from the original system (9), one has

$$\begin{cases} \dot{\boldsymbol{x}}_{\mathrm{r},k} - \dot{\boldsymbol{x}}_{\mathrm{r},k}^{\mathrm{p}} = \boldsymbol{A}_{\mathrm{r}} \left(\boldsymbol{x}_{\mathrm{r},k} - \boldsymbol{x}_{\mathrm{r},k}^{\mathrm{p}} \right) + \boldsymbol{B}_{\mathrm{r}} \left[\mathrm{sat}\left(\boldsymbol{u}_{\mathrm{r},k} \right) - \boldsymbol{u}_{\mathrm{r},k}^{\mathrm{p}} \right] \\ \boldsymbol{y}_{\mathrm{r},k} - \boldsymbol{y}_{\mathrm{r},k}^{\mathrm{p}} = \boldsymbol{C}_{\mathrm{r}} \left(\boldsymbol{x}_{\mathrm{r},k} - \boldsymbol{x}_{\mathrm{r},k}^{\mathrm{p}} \right), \boldsymbol{x}_{\mathrm{r},k}(0) - \boldsymbol{x}_{\mathrm{r},k}^{\mathrm{p}}(0) = \boldsymbol{0} \end{cases} \tag{13}$$

Then, by defining

$$\boldsymbol{x}_{\mathrm{r},k}^{\mathrm{s}} = \boldsymbol{x}_{\mathrm{r},k} - \boldsymbol{x}_{\mathrm{r},k}^{\mathrm{p}}, \boldsymbol{y}_{\mathrm{r},k}^{\mathrm{s}} = \boldsymbol{y}_{\mathrm{r},k} - \boldsymbol{y}_{\mathrm{r},k}^{\mathrm{p}}, \boldsymbol{u}_{\mathrm{r},k}^{\mathrm{s}} = \boldsymbol{u}_{\mathrm{r},k} - \boldsymbol{u}_{\mathrm{r},k}^{\mathrm{p}} \tag{14}$$

the system (13) becomes

$$\begin{cases} \dot{\boldsymbol{x}}_{\mathrm{r},k}^{\mathrm{s}} = \boldsymbol{A}_{\mathrm{r}} \boldsymbol{x}_{\mathrm{r},k}^{\mathrm{s}} + \boldsymbol{B}_{\mathrm{r}} \left[\mathrm{sat}\left(\boldsymbol{u}_{\mathrm{r},k}^{\mathrm{s}} + \boldsymbol{u}_{\mathrm{r},k}^{\mathrm{p}} \right) - \boldsymbol{u}_{\mathrm{r},k}^{\mathrm{p}} \right] \\ \boldsymbol{y}_{\mathrm{r},k}^{\mathrm{s}} = \boldsymbol{C}_{\mathrm{r}} \boldsymbol{x}_{\mathrm{r},k}^{\mathrm{s}}, \boldsymbol{x}_{\mathrm{r},k}^{\mathrm{s}}(0) = \boldsymbol{0} \end{cases} \tag{15}$$

which is a nonlinear system with input saturation. This is called the secondary system. According to Eq. (14), the state and the output satisfy

$$\boldsymbol{x}_{\mathrm{r},k} = \boldsymbol{x}_{\mathrm{r},k}^{\mathrm{s}} + \boldsymbol{x}_{\mathrm{r},k}^{\mathrm{p}}, \boldsymbol{y}_{\mathrm{r},k} = \boldsymbol{y}_{\mathrm{r},k}^{\mathrm{s}} + \boldsymbol{y}_{\mathrm{r},k}^{\mathrm{p}} \tag{16}$$

where $\boldsymbol{y}_{\mathrm{r},k}^{\mathrm{p}}$ and $\boldsymbol{x}_{\mathrm{r},k}^{\mathrm{s}}$ are estimated by an observer stated in Theorem 1. Eq. (16) implies that the sum of the two decomposed systems is equal to the original system.

Theorem 1. Suppose that an observer is designed to estimate $\mathbf{y}_{\mathrm{r},k}^{\mathrm{p}}$ and $\boldsymbol{x}_{\mathrm{r},k}^{\mathrm{s}}$ in Eq. (12) and Eq. (15) as follows:

$$\begin{cases} \dot{\hat{\boldsymbol{x}}}_{\mathrm{r},k}^{\mathrm{s}} = \boldsymbol{A}_{\mathrm{r}} \hat{\boldsymbol{x}}_{\mathrm{r},k}^{\mathrm{s}} + \boldsymbol{B}_{\mathrm{r}} \left[\mathrm{sat}\left(\boldsymbol{u}_{\mathrm{r},k} \right) - \boldsymbol{u}_{\mathrm{r},k}^{\mathrm{p}} \right] \\ \hat{\boldsymbol{y}}_{\mathrm{r},k}^{\mathrm{p}} = \boldsymbol{y}_{\mathrm{r},k} - \boldsymbol{C}_{\mathrm{r}} \hat{\boldsymbol{x}}_{\mathrm{r},k}^{\mathrm{s}} \end{cases} \quad \hat{\boldsymbol{x}}_{\mathrm{r},k}^{\mathrm{s}}(0) = \boldsymbol{0} \tag{17}$$

then $\hat{\boldsymbol{y}}_{\mathrm{r},k}^{\mathrm{p}} = \boldsymbol{y}_{\mathrm{r},k}^{\mathrm{p}}, \hat{\boldsymbol{x}}_{\mathrm{r},k}^{\mathrm{s}} = \boldsymbol{x}_{\mathrm{r},k}^{\mathrm{s}}$.

Proof. Subtracting Eq. (17) from Eq. (15) results in

$$\dot{\tilde{\boldsymbol{x}}}_{\mathrm{r},k}^{\mathrm{s}} = \boldsymbol{A}_{\mathrm{r}} \tilde{\boldsymbol{x}}_{\mathrm{r},k}^{\mathrm{s}}, \tilde{\boldsymbol{x}}_{\mathrm{r},k}^{\mathrm{s}}(0) = \boldsymbol{0} \tag{18}$$

where $\tilde{\boldsymbol{x}}_{\mathrm{r},k}^{\mathrm{s}} = \boldsymbol{x}_{\mathrm{r},k}^{\mathrm{s}} - \hat{\boldsymbol{x}}_{\mathrm{r},k}^{\mathrm{s}}$. Then, considering that $\boldsymbol{A}_{\mathrm{r}}$ is stable, $\tilde{\boldsymbol{x}}_{\mathrm{r},k}^{\mathrm{s}} \equiv \boldsymbol{0}$. That means $\hat{\boldsymbol{x}}_{\mathrm{r},k}^{\mathrm{s}} = \boldsymbol{x}_{\mathrm{r},k}^{\mathrm{s}}$. Consequently, $\hat{\boldsymbol{y}}_{\mathrm{r},k}^{\mathrm{p}} = \boldsymbol{y}_{\mathrm{r},k} - \boldsymbol{C}_{\mathrm{r}} \hat{\boldsymbol{x}}_{\mathrm{r},k}^{\mathrm{s}} = \boldsymbol{y}_{\mathrm{r},k}^{\mathrm{p}}$. □

If $\boldsymbol{y}_{\mathrm{r,d}}-\boldsymbol{y}_{\mathrm{r},k}^{\mathrm{p}}\equiv\boldsymbol{0}$, then $\left(\boldsymbol{x}_{\mathrm{r},k}^{\mathrm{s}},\boldsymbol{u}_{\mathrm{r},k}^{\mathrm{s}}\right)=\boldsymbol{0}$ is an equilibrium point of system (15). It is clear that if the controller $\boldsymbol{u}_{\mathrm{r},k}^{\mathrm{p}}$ drives $\boldsymbol{y}_{\mathrm{r},k}^{\mathrm{p}}\to\boldsymbol{y}_{\mathrm{r,d}}$ and the controller $\boldsymbol{u}_{\mathrm{r},k}^{\mathrm{s}}$ drives $\boldsymbol{y}_{\mathrm{r},k}^{\mathrm{s}}\to\boldsymbol{0}$ as $k\to\infty$, then $\boldsymbol{y}_{\mathrm{r},k}\to\boldsymbol{y}_{\mathrm{r,d}}$, as $k\to\infty$. The strategy here is to assign the tracking task to the primary system (12) and the stabilization task to the secondary system (15), respectively. According to these, the ASD offers a way to simplify the original control problem.

So far, the considered system is decomposed into two systems in charge of corresponding tasks. In the following, controller design in the form of problems is proposed with respect to the two component tasks, respectively.

3.1.2. Problem 1: tracking problem for the primary system

For system (12), design an ILC controller

$$\boldsymbol{u}_{\mathrm{r},k+1}^{\mathrm{p}}=\boldsymbol{u}_{\mathrm{r},k}^{\mathrm{p}}+\mathcal{H}\hat{\boldsymbol{e}}_{\mathrm{r},k}^{\mathrm{p}} \tag{19}$$

such that $\left\|\tilde{\boldsymbol{u}}_{\mathrm{r},k}^{\mathrm{p}}\right\|_{\mathcal{L}_2[0,T]}\to0,\left\|\boldsymbol{e}_{\mathrm{r},k}^{\mathrm{p}}\right\|_{\mathcal{L}_2[0,T]}\to0,\left\|\boldsymbol{e}_{\mathrm{r},k}^{\mathrm{p}}\right\|_{\mathcal{L}_\infty[0,T]}\to0$ as $k\to\infty$, where $\mathcal{H}:\mathcal{L}_2[0,T]\mapsto\mathcal{L}_2[0,T]$ is a linear operator, and $\hat{\boldsymbol{e}}_{\mathrm{r},k}^{\mathrm{p}}=\boldsymbol{y}_{\mathrm{r,d}}-\hat{\boldsymbol{y}}_{\mathrm{r},k}^{\mathrm{p}},\tilde{\boldsymbol{u}}_{\mathrm{r},k}^{\mathrm{p}}=\boldsymbol{u}_{\mathrm{r,d}}-\boldsymbol{u}_{\mathrm{r},k}^{\mathrm{p}}$.

Theorem 2. Suppose that the operator of the receiver is denoted as $\mathcal{G}_{\mathrm{r}}$, the ILC controller for system (12) is designed as

$$\begin{cases}\boldsymbol{u}_{\mathrm{r},k+1}^{\mathrm{p}}=\boldsymbol{u}_{\mathrm{r},k}^{\mathrm{p}}+\alpha_k\mathcal{G}_{\mathrm{r}}^{*}\hat{\boldsymbol{e}}_{\mathrm{r},k}^{\mathrm{p}}\\ \boldsymbol{u}_{\mathrm{r},1}^{\mathrm{p}}=\boldsymbol{u}_{\mathrm{r,dock}}\end{cases} \tag{20}$$

where $\dfrac{b_k-\sqrt{(b_k)^2-(1-\rho_k)a_kc_k}}{a_k}\le\alpha_k\le\dfrac{b_k+\sqrt{(b_k)^2-(1-\rho_k)a_kc_k}}{a_k}$, $\rho_k\in\left[1-\dfrac{(b_k)^2}{a_kc_k},1\right)$ with $a_k=\left\|\mathcal{G}^{*}\boldsymbol{e}_{\mathrm{r},k}^{\mathrm{p}}\right\|_{\mathcal{L}_2[0,T]}^2$, $b_k=\left\|\boldsymbol{e}_{\mathrm{r},k}^{\mathrm{p}}\right\|_{\mathcal{L}_2[0,T]}^2$, $c_k=\left\|\tilde{\boldsymbol{u}}_{\mathrm{r},k}^{\mathrm{p}}\right\|_{\mathcal{L}_2[0,T]}^2$, $\mathcal{G}_{\mathrm{r}}:\mathcal{L}_2[0,T]\mapsto\mathcal{L}_2[0,T]$ is defined as $\mathcal{G}_{\mathrm{r}}\boldsymbol{u}=\int_0^t\boldsymbol{C}_{\mathrm{r}}\mathrm{e}^{\boldsymbol{A}_{\mathrm{r}}(t-\tau)}\boldsymbol{B}_{\mathrm{r}}\boldsymbol{u}(\tau)\mathrm{d}\tau$, then $\left\|\tilde{\boldsymbol{u}}_{\mathrm{r},k}^{\mathrm{p}}\right\|_{\mathcal{L}_2[0,T]}\to0,\left\|\boldsymbol{e}_{\mathrm{r},k}^{\mathrm{p}}\right\|_{\mathcal{L}_2[0,T]}\to0,\left\|\boldsymbol{e}_{\mathrm{r},k}^{\mathrm{p}}\right\|_{\mathcal{L}_\infty[0,T]}\to0$ as $k\to\infty$, $\boldsymbol{u}_{\mathrm{r,dock}}$ denotes the initial input that comes from historical experience (previous tasks) or a theoretical method. In particular, if

$$\alpha_k=\frac{b_k}{a_k},\ \text{when}\ \rho_k=1-\frac{(b_k)^2}{a_kc_k} \tag{21}$$

then $\left\|\tilde{\boldsymbol{u}}_{\mathrm{r},k}^{\mathrm{p}}\right\|_{\mathcal{L}_2[0,T]}$ converges fastest.

Proof. Please refer to Ref.[28] for the detailed proof. □

3.1.3. Problem 2: Stabilization control problem for the secondary system

For system (15), design a stabilization controller

$$\boldsymbol{u}_{\mathrm{r},k+1}^{\mathrm{s}}=\boldsymbol{l}\hat{\boldsymbol{x}}_{\mathrm{r},k+1}^{\mathrm{s}} \tag{22}$$

satisfying that $\left\|\boldsymbol{x}_{\mathrm{r},k}^{\mathrm{s}}\right\|_{\mathcal{L}_\infty[0,T]}\to0$, when $\left\|\tilde{\boldsymbol{u}}_{\mathrm{r},k}^{\mathrm{p}}\right\|_{\mathcal{L}_2[0,T]}\to0,\left\|\boldsymbol{e}_{\mathrm{r},k}^{\mathrm{p}}\right\|_{\mathcal{L}_2[0,T]}\to0$.

In fact, if Problem 1 is well solved, then Problem 2 will be solved indirectly by Theorem 3.

Theorem 3. For system (15), suppose that the controller $\boldsymbol{u}_{\mathrm{r},k+1}^{\mathrm{s}}$ is designed as Eq. (22). Then, $\left\|\boldsymbol{x}_{\mathrm{r},k}^{\mathrm{s}}\right\|_{\mathcal{L}_\infty[0,T]}\to0$ as $\left\|\tilde{\boldsymbol{u}}_{\mathrm{r},k}^{\mathrm{p}}\right\|_{\mathcal{L}_2[0,T]}\to0,\left\|\boldsymbol{e}_{\mathrm{r},k}^{\mathrm{p}}\right\|_{\mathcal{L}_2[0,T]}\to0$.

Proof. See Ref.[28]. □

With the solutions to the two problems in hand, one is ready to claim Theorem 4.

Theorem 4. Under Assumptions 1- 2, suppose (A) Problems 1 and 2 are solved; (B) the controller for system (9) is designed as

$$\begin{aligned}&\text{Controller}\begin{cases}\boldsymbol{u}_{\mathrm{r},k+1}=\boldsymbol{u}_{\mathrm{r},k}^{\mathrm{p}}+\alpha_k\mathcal{G}_{\mathrm{r}}^{*}\hat{\boldsymbol{e}}_{\mathrm{r},k}^{\mathrm{p}}+\boldsymbol{l}\hat{\boldsymbol{x}}_{\mathrm{r},k+1}^{\mathrm{s}}\\ \boldsymbol{u}_{\mathrm{r},1}=\boldsymbol{u}_{\mathrm{r,dock}}\end{cases}\\ &\text{Obsever}\begin{cases}\dot{\hat{\boldsymbol{x}}}_{\mathrm{r},k}^{\mathrm{s}}=\boldsymbol{A}_{\mathrm{r}}\hat{\boldsymbol{x}}_{\mathrm{r},k}^{\mathrm{s}}+\boldsymbol{B}_{\mathrm{r}}\left[\mathrm{sat}\left(\boldsymbol{u}_{\mathrm{r},k}\right)-\boldsymbol{u}_{\mathrm{r},k}^{\mathrm{p}}\right] & \hat{\boldsymbol{x}}_{\mathrm{r},k}^{\mathrm{s}}\left(0\right)=\boldsymbol{0}\\ \hat{\boldsymbol{y}}_{\mathrm{r},k}^{\mathrm{p}}=\boldsymbol{y}_{\mathrm{r},k}-\boldsymbol{C}_{\mathrm{r}}\hat{\boldsymbol{x}}_{\mathrm{r},k}^{\mathrm{s}}\end{cases}\end{aligned}\tag{23}$$

Then, the tracking error of system (9) satisfies $\left\|\boldsymbol{e}_{\mathrm{r},k}\right\|_{\mathcal{L}_\infty[0,T]}\to 0$ as $k\to\infty$.

Proof. Under condition (A), by using the ε-δ definition, it can be obtained that

$$\left\|\boldsymbol{e}_{\mathrm{r},k}\right\|_{\mathcal{L}_\infty[0,T]}\le\left\|\boldsymbol{e}_{\mathrm{r},k}^{\mathrm{p}}\right\|_{\mathcal{L}_\infty[0,T]}+\left\|\boldsymbol{e}_{\mathrm{r},k}^{\mathrm{s}}\right\|_{\mathcal{L}_\infty[0,T]}\to 0\ \text{as}\ k\to\infty\tag{24}$$

According to Theorem 1, observer Eq.(17) will make $\hat{\boldsymbol{y}}_{\mathrm{r},k}^{\mathrm{p}}=\boldsymbol{y}_{\mathrm{r},k}^{\mathrm{p}}$, $\hat{\boldsymbol{x}}_{\mathrm{r},k}^{\mathrm{s}}=\boldsymbol{x}_{\mathrm{r},k}^{\mathrm{s}}$. Thus, the controller (23) guarantees $\left\|\boldsymbol{e}_{\mathrm{r},k}\right\|_{\mathcal{L}_\infty[0,T]}\to 0$ as $k\to\infty$. □

3.2. Correction algorithm based on adjoint operator

The receiver-related uncertainties can be diminished by controller (23). However, this is not the case for receiver -independent uncertainties. In this part, the receiver-independent uncertainties are considered. Because of the strong nonlinearity of the drogue, the iteration by using the drogue error may not achieve tracking convergence, and is likely to make the receiver oscillate along with the last error, which is unacceptable. Thus, the designed correction term will not iterate. For the integrated system (6), ignoring the nonlinear part, the according operator is defined as $\mathcal{G}_{\mathrm{a}}$.

By utilizing the relative position error of the probe and the drogue at the docking moment, namely $-\boldsymbol{p}_{\mathrm{d/p},k}\left(t_{\mathrm{dock}}\right)$, a correction term is designed as

$$\Delta\boldsymbol{u}_{\mathrm{r},k+1}=\alpha_k'\mathcal{G}_{\mathrm{a}}^{*}\boldsymbol{e}_{\mathrm{d/p},k}\tag{25}$$

where $\boldsymbol{e}_{\mathrm{d/p},k}\left(t\right)=-\boldsymbol{p}_{\mathrm{d/p},k}\left(t_{\mathrm{end}}\right)\left(t\in[0,T]\right)$, $\mathcal{G}_{\mathrm{a}}^{*}$ is the adjoint operator of $\mathcal{G}_{\mathrm{a}}$.

3.3. Controller integration

Finally, by integrating the controller (23) and the correction term Eq.(25), the complete controller is given as

$$\begin{aligned}&\text{Controller}\begin{cases}\boldsymbol{u}_{\mathrm{r},k+1}=\boldsymbol{u}_{\mathrm{r},k+1}^{\mathrm{p}}+\boldsymbol{u}_{\mathrm{r},k+1}^{\mathrm{s}}+\Delta\boldsymbol{u}_{\mathrm{r},k+1}=\boldsymbol{u}_{\mathrm{r},k}^{\mathrm{p}}+\alpha_k\mathcal{G}_{\mathrm{r}}^{*}\hat{\boldsymbol{e}}_{\mathrm{r},k}^{\mathrm{p}}+\boldsymbol{l}\hat{\boldsymbol{x}}_{k+1}^{\mathrm{s}}+\alpha_k'\mathcal{G}_{\mathrm{a}}^{*}\boldsymbol{e}_{\mathrm{d/p},k}\\ \boldsymbol{u}_{\mathrm{r},1}=\boldsymbol{u}_{\mathrm{r,dock}}\end{cases}\\ &\text{Obsever}\begin{cases}\dot{\hat{\boldsymbol{x}}}_{\mathrm{r},k}^{\mathrm{s}}=\boldsymbol{A}_{\mathrm{r}}\hat{\boldsymbol{x}}_{\mathrm{r},k}^{\mathrm{s}}+\boldsymbol{B}_{\mathrm{r}}\left[\mathrm{sat}\left(\boldsymbol{u}_{\mathrm{r},k}\right)-\boldsymbol{u}_{\mathrm{r},k}^{\mathrm{p}}\right] & \hat{\boldsymbol{x}}_{\mathrm{r},k}^{\mathrm{s}}\left(0\right)=\boldsymbol{0}\\ \hat{\boldsymbol{y}}_{\mathrm{r},k}^{\mathrm{p}}=\boldsymbol{y}_{\mathrm{r},k}-\boldsymbol{C}_{\mathrm{r}}\hat{\boldsymbol{x}}_{\mathrm{r},k}^{\mathrm{s}}\end{cases}\end{aligned}\tag{26}$$

Noteworthy, $\boldsymbol{u}_{\mathrm{r},k+1}^{\mathrm{s}},\Delta\boldsymbol{u}_{\mathrm{r},k+1}$ do not iterate, and so the final controller is composed of an iterative feedforward part from the primary system, an online feedback part from the secondary system, and a non-iterative feedforward correction part. The outline of the ILC control scheme used in this work is shown in Fig. 4. The designed iterative learning controller works online. After each docking attempt, the controller adjusts the control input once.

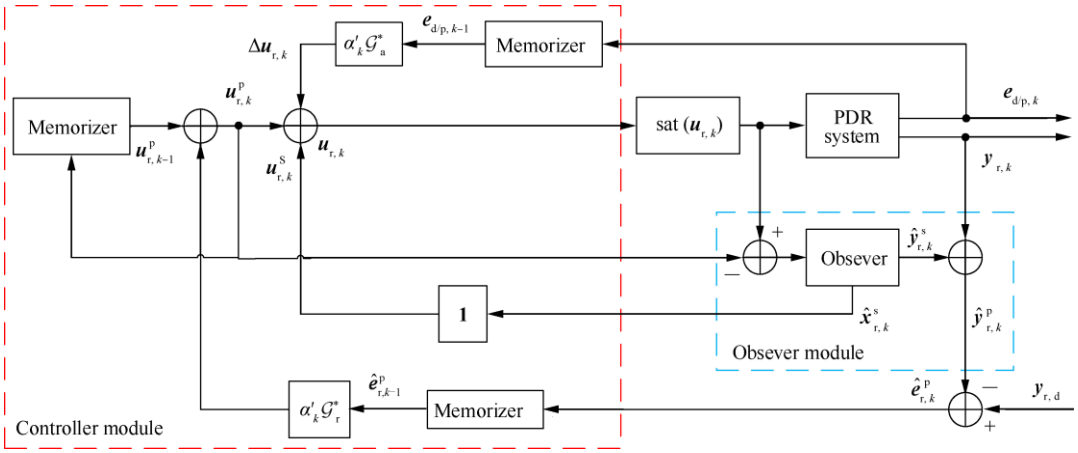

Fig. 4 Controller overview.

4. Simulation results

In this section, the effectiveness, robustness, and practicality of the proposed control method are demonstrated through simulations and analyses.

4.1. System information

A MATLAB/SIMULINK based simulation environment with a three-dimensional virtual-reality display shown in Fig. 5 has been developed by the authors' research lab to simulate the docking stage of PDR. The detailed information about the modeling procedure, model parameters, and simulation environment can refer to Ref. [29,36]. Noteworthy, although the drogue dynamics Eq.(4) is considered in the controller design, the link-connected model of the hose-drogue system is adopted in the simulation environment. A Hose-Drum Unit (HDU) is also included to improve the fitness of the simulation model.

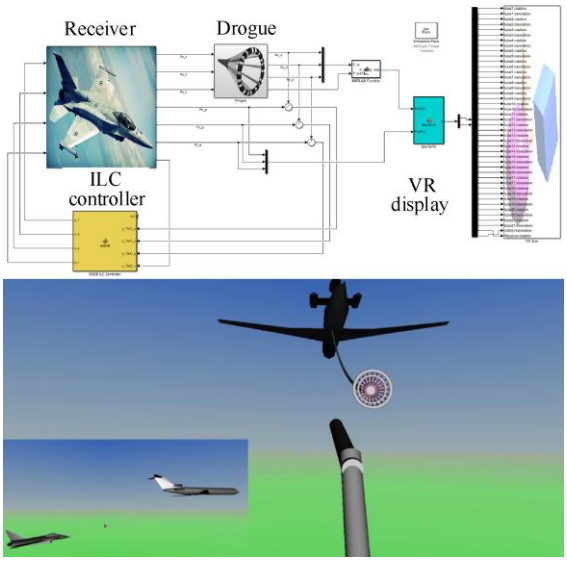

Fig. 5 MATLAB/SIMULINK based simulation environment with a three-dimensional virtual-reality display.

The effect of the system uncertainty and disturbance among different tasks is considered by the following three ways:

1) Add uncertainties to the actuators by multiplying actuator inputs by a factor of 1.4.

2) The actual bow wave effect is changed to 1.3 times of the modeled bow wave effect.

3) Add a side wind disturbance to the atmospheric environment, which primarily acts on the hose-drogue model.

The uncertainty 1) is a receiver-related uncertainty, while uncertainties 2) and 3) are receiver-independent uncertainties. Noteworthy, the aforementioned three changes just apply to the plant, while controller design is still based on the model built previously.

We aim to propose a fast adjustment strategy, and so just the first two or three iterations are focused. Namely, the reference input is injected to the receiver in the first iteration, after which, the output error is obtained by subtracting the system output from the reference output. Then, the second input is given by our controller (26) to achieve a successful docking. The ILC controller parameters used in the simulation are set as $\alpha_k = \left\|\hat{\boldsymbol{e}}_{\mathrm{r},k}^{\mathrm{p}}\right\|_{\mathcal{L}_2[0,T]}^2 \Big/ \left\|\mathcal{G}^*\hat{\boldsymbol{e}}_{\mathrm{r},k}^{\mathrm{p}}\right\|_{\mathcal{L}_2[0,T]}^2$, $\alpha_k' = \left\|\boldsymbol{e}_{\mathrm{d/p},k}\right\|_{\mathcal{L}_2[0,T]}^2 \Big/ \left\|\mathcal{G}_{\mathrm{a}}^*\boldsymbol{e}_{\mathrm{d/p},k}\right\|_{\mathcal{L}_2[0,T]}^2$, and $\mathbf{l}$ is determined by the pole placement method as

$$\mathbf{l} = 10^3 \begin{bmatrix} 0.0046 & 0.0010 & -0.0724 & -0.0003 & 0.0575 & -0.0010 & 0.0031 & 0.7009 & -0.0526 & 0.5865 & -0.0028 & 0.1090 \\ 0.0012 & 0.0014 & -0.0997 & 0.0007 & 0.0797 & -0.0043 & -0.0037 & -0.9161 & 0.0588 & -1.1962 & -0.0026 & -0.1783 \\ -0.0014 & 0.0002 & -0.1369 & -0.0010 & 0.0960 & -0.0175 & 0.0094 & 1.9114 & -0.1407 & 1.8364 & -0.0019 & 0.2944 \end{bmatrix}^{\mathrm{T}}.$$

4.2. Two existing methods for comparison

As baseline controllers to be compared with, two traditional ILC controllers are briefly introduced. One is a classical Derivative-type (D-type) ILC controller, and the other is an adjoint-type ILC controller, which is similar to the ILC controller for the primary system in this paper.

4.2.1. D-type iterative learning control

A D-type iterative learning controller is designed as

$$\boldsymbol{u}_{\mathrm{r},k+1} = \boldsymbol{u}_{\mathrm{r},k} + p\dot{\boldsymbol{e}}_{\mathrm{r},k} \tag{27}$$

where $p = -0.2$ is selected.

4.2.2. Adjoint-type iterative learning control

Because the ILC controller for the primary system is similar to the controller designed in Ref.[25], the controller in Ref.[25] is employed for comparison. In this method, the nonlinear system is directly linearized, and then the learning law is designed based on the adjoint operator. Thus, by neglecting the saturation constraint of system (9), one has

$$\begin{cases} \dot{\boldsymbol{x}}_{\mathrm{r},k}(t) = \boldsymbol{A}_{\mathrm{r}}\boldsymbol{x}_{\mathrm{r},k}(t) + \boldsymbol{B}_{\mathrm{r}}\boldsymbol{u}_{\mathrm{r},k}(t) \\ \boldsymbol{y}_{\mathrm{r},k}(t) = \boldsymbol{C}_{\mathrm{r}}\boldsymbol{x}_{\mathrm{r},k}(t) \end{cases} \qquad \boldsymbol{x}_{\mathrm{r},k}(0) = \boldsymbol{x}_{\mathrm{r},0}; t \in [0,T] \tag{28}$$

Then, the adjoint-type ILC controller is designed as

$$\boldsymbol{u}_{\mathrm{r},k+1} = \boldsymbol{u}_{\mathrm{r},k} + \alpha\mathcal{G}_l^*\boldsymbol{e}_{\mathrm{r},k} \tag{29}$$

Where $\mathcal{G}_l$ is the corresponding operator of system (28), α is a constant which does not change with k, and it is chosen as $\alpha = 50$ in the simulation. The adjoint operator $\mathcal{G}_l^*: \mathcal{L}_2[0,T] \mapsto \mathcal{L}_2[0,T]$ is calculated as follows [25,26]

$$\mathcal{G}_l^*\boldsymbol{u} = \int_t^T \boldsymbol{B}_{\mathrm{r}}^{\mathrm{T}} \mathrm{e}^{-\boldsymbol{A}_{\mathrm{r}}^{\mathrm{T}}(t-\tau)} \boldsymbol{C}_{\mathrm{r}}^{\mathrm{T}} \boldsymbol{u}(\tau)\,\mathrm{d}\tau \tag{30}$$

4.3. Simulation results

The convergence of the terminal docking error of different control methods is compared in Fig. 6. Because $r_{\mathrm{d}} = 0.305$ as shown in Fig. 3 (b), a docking attempt is regarded as successful if the docking error e_{dock} is less than 0.3. The docking error at the docking moment t_{dock} is summarized in Table 2. Compared with two traditional TILC controllers, the proposed ASDB ILC controller gives the highest convergence speed under uncertainties. Although the classical D-type ILC controller can deal with the NMP systems in theory, its convergence process is extremely slow and unacceptable. The docking error cannot satisfy the precision requirement. In addition, the adjoint-type ILC has a higher convergence speed than that of the D-type ILC. Noteworthy, for the three controllers, the controller parameters

are selected carefully. If smaller parameters are selected, the convergence speed will decrease. If larger parameters are selected, the system oscillation will occur. Both of them will lead to worse convergence of the terminal docking error.

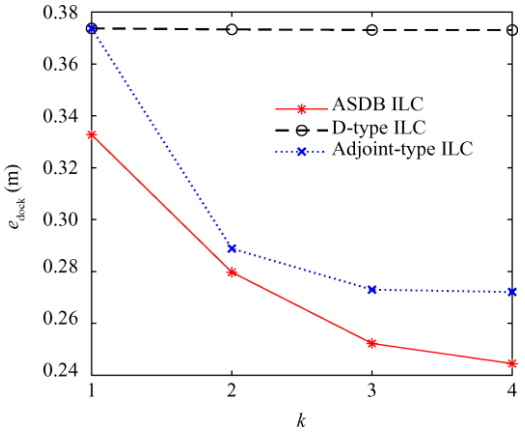

Fig. 6 Comparison of the convergence of the terminal docking error of different control methods..

Table 2 Docking errors of different control methods

Control method	Docking error		
	1st attempt	2nd attempt	3rd attempt
ASDB ILC	0.3327	0.2797	0.2522
D-type ILC	0.3737	0.3733	0.3731
Adjoint-type ILC	0.3737	0.2888	0.2730

For ASDB ILC, the receiver position during the docking process is depicted in Fig. 7, and the relative position and relative velocity between the drogue and the probe are shown in Fig. 8. It can be observed from Fig. 8 that the relative position and relative velocity between the drogue and the probe approach quickly to the reference trajectory, which further reduces the docking error. Noteworthy, the oscillations in Fig. 8 are mainly caused by the drogue, and the oscillation of the receiver is small, which can be verified by Fig. 7. The proposed fast adjustment strategy can deal with various uncertainties and achieve a successful docking in the second docking attempt. The fast adjustment among different tasks can be accomplished.

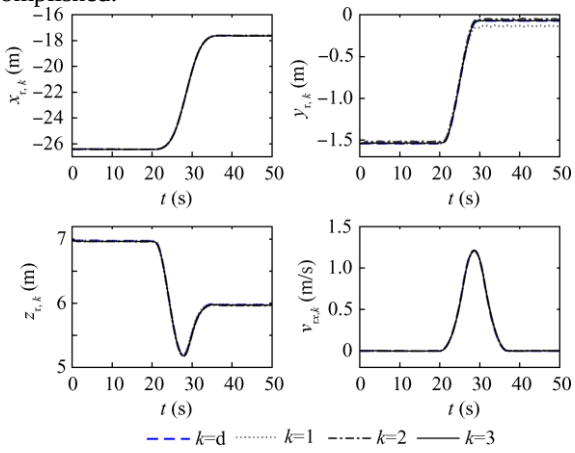

Fig. 7 Receiver position during docking process (k = d denotes the reference trajectory).

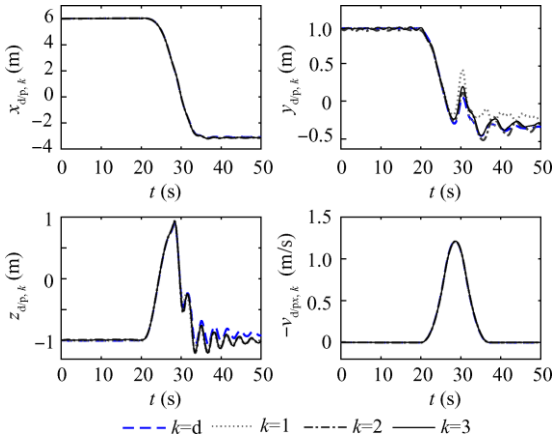

Fig. 8 Relative position and velocity between drogue and probe during docking process.

In order to further verify the robustness of the controller, atmospheric turbulence disturbance is taken into consideration by adding the Dryden wind-turbulence model to the PDR system. The designed ASDB ILC controller can still achieve a successful docking in the second docking attempt, as shown in Fig. 9.

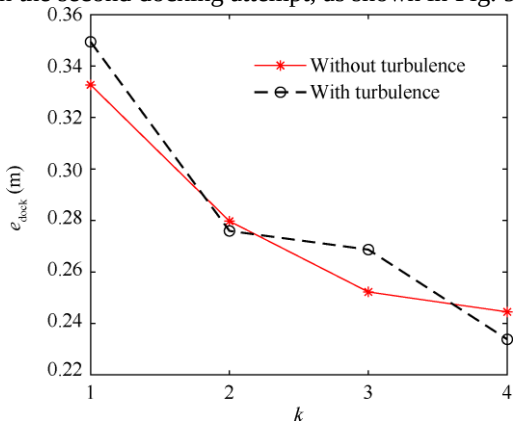

Fig. 9 Comparison of convergence of terminal docking error with and without turbulence disturbance.

5. Conclusions

An additive-state-decomposition-based output feedback iterative learning control method for probe-drogue refueling was introduced. It was shown that ASD could be used to separate NMP feature form input saturation and nonlinearity by dividing the original system into a primary system and a secondary system. Adjoint-type ILC was executed for the LTI primary system, and state feedback was utilized to stabilize the nonlinear secondary system. Furthermore, a non-iterative correction algorithm based on adjoint operator was proposed to compensate for the receiver -independent uncertainties. Simulation results show the promising performance of the ASDB ILC, which outperforms traditional D-type ILC and adjoint-type ILC in the docking control of PDR. ASDB ILC has good tracking effect and high convergence speed under multiple uncertainties. The immediate extension of this work is to integrate it with system identification. Based on the nonlinear model of bow wave effect from system identification, ASDB ILC can achieve better control performance.

Acknowledgement

This work was supported by the National Natural Science Foundation of China (No.: 61473012).

References

1. Thomas PR, Bhandari U, Bullock S, Richardson TS, Du Bois JL. Advances in air to air refuelling. *Prog Aerosp Sci* 2014; 71: 14–35.

2. Nalepka JP, Hinchman, JL. Automated aerial refueling: Extending the effectiveness of unmanned air vehicles. *AIAA modeling and simulation technologies conference and exhibit*; 2005 Aug 15-18; San Francisco, USA. Reston: AIAA; 2005.
3. Bhandari U, Thomas PR, Bullock S, Richardson TS, Du Bois J. Bow wave effect in probe-and-drogue aerial refuelling. *AIAA guidance, navigation, and control conference*; 2013 Aug 19-22; Boston, USA. Reston: AIAA; 2013.
4. NATO. Air-to-Air Refuelling. Brussels, Belgium: NATO; 2010. Report No.: ATP-56(B).
5. Tandale MD, Bowers R, Valasek J. Trajectory tracking controller for vision-based probe and drogue autonomous aerial refueling. *J Guidance Control Dyn* 2006; **29**(4): 846–57.
6. Fravolini ML, Ficola A, Campa G, Napolitano MR, Seanor B. Modeling and control issues for autonomous aerial refueling for UAVs using a probe-drogue refueling system. *Aerosp Sci Technol* 2004; **8**(7): 611–8.
7. Valasek J, Gunnam K, Kimmett J, Junkins JL, Hughes D, Tandale MD. Vision-based sensor and navigation system for autonomous air refueling. *J Guidance Control Dyn* 2005; **28**(5): 979–89.
8. Kimmett J, Valasek J, Junkins JL. Vision based controller for autonomous aerial refueling. *Proceeings of the 2002 international conference on control applications IEEE*; 2002 Sep 18-20; Glasgow, UK. Pascataway: IEEE Press; 2002. p. 1138–43.
9. Su Z, Wang H, Shao X, Yao P. Autonomous aerial refueling precise docking based on active disturbance rejection control. *IECON 2015-41st annual conference of the IEEE industrial electronics society*; 2015 Nov 9-12; Yokohama, Japan. Pascataway: IEEE Press; 2015. p. 4574–8.
10. Wang J, Patel VV, Cao C, Hovakimyan N, Lavretsky E. Verifiable L1 adaptive controller for aerial refueling. *AIAA guidance, navigation and control conference and exhibit*; 2007 Aug 20-23; Hilton Head, USA. Reston: AIAA; 2007.p.1-23.
11. Valasek J, Famularo D, Marwaha M. Fault-tolerant adaptive model inversion control for vision-based autonomous air refueling. *J Guidance Control Dyn* 2017; **40**(6): 1336–47.
12. Wang H, Dong X, Xue J, Liu J. Dynamic modeling of a hose-drogue aerial refueling system and integral sliding mode backstepping control for the hose whipping phenomenon. *Chin J Aeronaut* 2014; **27**(4): 930–46.
13. Su Z, Wang H, Li N, Yu Y, Wu J. Exact docking flight controller for autonomous aerial refueling with back-stepping based high order sliding mode. *Mechanical Syst Signal Process* 2018; 101: 338-60.
14. Ahn HS, Chen YQ, Moore KL. Iterative learning control: Brief survey and categorization. *IEEE Trans on Syst Man Cybernetics, Part C (Applications and Reviews)* 2007; **37**(6): 1099-121.
15. Dai XH, Quan Q, Ren JR, Xi ZY, Cai KY. Terminal iterative learning control for autonomous aerial refueling under aerodynamic disturbances. *J Guidance Control Dyn* 2018; **41**(7): 1577-84.
16. Sogo T. On the equivalence between stable inversion for nonminimum phase systems and reciprocal transfer functions defined by the two-sided Laplace transform. *Automatica* 2010; **46**(1): 122-6.
17. Devasia S, Chen D, Paden B. Nonlinear inversion-based output tracking. *IEEE Trans Autom Control* 1996; **41**(7): 930-42.
18. Hunt LR, Meyer G. Stable inversion for nonlinear systems. *Automatica* 1997; **33**(8): 1549-54.
19. Kinosita K, Sogo T, Adachi N. Iterative learning control using adjoint systems and stable inversion. *Asian J Control* 2002; **4**(1): 60-7.
20. Amann N, Owens DH, Rogers E. Iterative learning control for discrete-time systems with exponential rate of convergence. *IEE Proc-Control Theory Applications* 1996; **143**(2): 217-24.
21. Amann N, Owens DH, Rogers E. Iterative learning control using optimal feedback and feedforward actions. *Int J Control* 1996; **65**(2): 277-93.
22. Ghosh J, Paden B. A pseudoinverse-based iterative learning control. *IEEE Trans Autom Control* 2002; **47**(5): 831-7.
23. Chu B, Owens DH. Iterative learning control for constrained linear systems. *Int J Control* 2010; **83**(7):1397–413.
24. Liu S, Wu TJ. Robust iterative learning control design based on gradient method. *IFAC Proc Volumes* 2004; **37**(1): 613-8.
25. Sogo T, Kinoshita K, Adachi N. Iterative learning control using adjoint systems for nonlinear non-minimum phase systems. *Proceedings of the 39th IEEE conference on decision and control*; 2000 Dec 12-15; Sydney, Australia. Pascataway: IEEE Press; 2000. p. 3445-6.
26. Ogoshi R, Sogo T, Adachi N. Adjoint-type iterative learning control for nonlinear nonminimum phase system. *SICE annual conference program and abstracts SICE Annual conference*; 2002 Aug 5-7; Osaka, Japan. Pascataway: IEEE Press; 2002. p. 1547-50.
27. Quan Q, Cai KY, Lin H. Additive-state-decomposition-based tracking control framework for a class of nonminimum phase systems with measurable nonlinearities and unknown disturbances. *Int J Robust Nonlinear Control* 2015; **25**(2): 163-78.
28. Wei ZB, Quan Q, Cai KY. Output feedback ILC for a class of nonminimum phase nonlinear systems with input saturation: An additive-state-decomposition-based method. *IEEE Trans Autom Control* 2017; **62**(1): 502–8.
29. Wei ZB, Dai XH, Quan Q, Cai KY. Drogue dynamic model under bow wave in probe-and-drogue refueling. *IEEE Trans Aerosp Electron Syst* 2016; **52**(4): 1728-42.
30. Stepanyan V, Lavretsky E, Hovakimyan N. Aerial refueling autopilot design methodology: Application to F-16 aircraft model. *AIAA guidance, navigation, and control conference and exhibit*; 2004 Aug 16-19; Providence, Rhode Island. Reston: AIAA; 2004.p.1-11.

31. Meng D, Li W, Bangfeng W. Vision-based estimation of relative pose in autonomous aerial refueling. *Chin J Aeronaut* 2011; **24**(6): 807-15.
32. Wang X, Kong X, Zhi J, Chen Y, Dong X. Real-time drogue recognition and 3D locating for UAV autonomous aerial refueling based on monocular machine vision. *Chin J Aeronaut* 2015; **28**(6): 1667-75.
33. Fravolini M, Ficola A, Napolitano M, Campa G, Perhinschi M. Development of modeling and control tools for aerial refueling for UAVs. *AIAA guidance, navigation, and control conference and exhibit*; 2003 Aug 11-14; Austin, USA. Reston: AIAA; 2003.p.1-10.
34. Ochi Y, Kominami T. Flight control for automatic aerial refueling via PNG and LOS angle control. *AIAA guidance, navigation, and control conference and exhibit*; 2005 Aug 15-18, San Francisco, USA. Reston: AIAA; 2005.p.1-11.
35. Quan Q, Cai KY. Additive-state-decomposition-based tracking control for TORA benchmark. *J Sound Vib* 2013; **332**(20): 4829-41.
36. Dai XH, Wei ZB, Quan Q. Modeling and simulation of bow wave effect in probe and drogue aerial refueling. *Chin J Aeronaut* 2016; **29**(2): 448-61.